Engineering 13 (2022) 153–163

Contents lists available at ScienceDirect

Engineering

journal homepage: www.elsevier.com/locate/eng

Research
Bioreaction Engineering—Article

Mass Transfer, Gas Holdup, and Kinetic Models of Batch and Continuous Fermentation in a Novel Rectangular Dynamic Membrane Airlift Bioreactor

Ganlu Li [a,#], Kequan Chen [a,#], Yanpeng Wei [a], Jinlei Zeng [a], Yue Yang [a], Feng He [b], Hui Li [a,*], Pingkai Ouyang [a]

[a] College of Biotechnology and Pharmaceutical Engineering, Nanjing Tech University, Nanjing 211816, China
[b] Jiangsu Jicui Industrial Biotechnology Research Institute Co., Ltd., Nanjing 211800, China

ARTICLE INFO

Article history:
Received 2 February 2021
Revised 28 May 2021
Accepted 25 July 2021
Available online 10 December 2021

Keywords:
Airlift bioreactor
Dynamic membrane
Kinetic model
Batch fermentation
Continuous fermentation

ABSTRACT

Compared with conventional cylinder airlift bioreactors (CCABs) that produce coarse bubbles, a novel rectangular dynamic membrane airlift bioreactor (RDMAB) developed in our lab produces fine bubbles to enhance the volumetric oxygen mass transfer coefficient (k_La) and gas holdup, as well as improve the bioprocess in a bioreactor. In this study, we compared mass transfer, gas holdup, and batch and continuous fermentation for RNA production in CCAB and RDMAB. In addition, unstructured kinetic models for microbial growth, substrate utilization, and RNA formation were established. In batch fermentation, biomass, RNA yield, and substrate utilization in the RDMAB were higher than those in the CCAB, which indicates that dynamic membrane aeration produced a high k_La by fine bubbles; a higher k_La is more beneficial to aerobic fermentation. The starting time of continuous fermentation in the RDMAB was 20 h earlier than that in the CCAB, which greatly improved the biological process. During continuous fermentation, maintaining the same dissolved oxygen level and a constant dilution rate, the biomass accumulation and RNA concentration in the RDMAB were 9.71% and 11.15% higher than those in the CCAB, respectively. Finally, the dilution rate of RDMAB was 16.7% higher than that of CCAB during continuous fermentation while maintaining the same air aeration. In summary, RDMAB is more suitable for continuous fermentation processes. Developing new aeration and structural geometry in airlift bioreactors to enhance k_La and gas holdup is becoming increasingly important to improve bioprocesses in a bioreactor.

1. Introduction

Airlift bioreactors are commonly used in bioprocessing to produce a variety of chemicals, enzymes, and medicines because of their unique characteristics, such as ease of operation, low energy consumption, low shear stress, and simple mechanical geometry [1–3]. It has been reported that the internal loop airlift bioreactor is a more suitable fermentation apparatus and process for the growth of *Rhodotorula glutinis* than the conventional agitation bioreactor [4]. Conventional airlift bioreactors, which use porous plates, perforated pipes, orifices, or static membranes as the aeration unit, produce coarse bubbles, which lead to a low volumetric oxygen mass transfer coefficient (k_La) and low gas utilization efficiency; therefore, they require high aeration rates to meet the oxygen demands of microorganisms [5–7]. The production of biomass and lipids by an oleaginous yeast strain and the use of glycerol from biodiesel production as the substrate in agitation and airlift bioreactors has shown that high biomass and lipid yields can be achieved in a 3.0 L airlift bioreactor under uncontrolled pH regimes. However, high aeration rates still cannot meet the required oxygen demand, so pure oxygen needs to be flushed into the airlift bioreactor to maintain the fermentation process [8]. Li et al. [9] developed a new dynamic membrane that produces fine bubbles to enhance the k_La and yield of the product in a bioreactor. Thus, developing new aeration geometries in airlift bioreactors to reduce the bubble size and improve k_La is increasingly important to improve the bioprocess.

* Corresponding author.
E-mail address: lihui11@njtech.edu.cn (H. Li).
# The authors contributed equally to this work.

https://doi.org/10.1016/j.eng.2021.07.025

Ribonucleic acid (RNA), a very important macromolecule produced during gene expression in living organisms, can be hydrolyzed to yield individual nucleotides [10,11]. RNA and its hydrolysate nucleotides have a variety of physiological functions, such as enhancing immune function and improving self-repair, anti-aging, and antiviral activities [12–14]. RNA and its hydrolysate nucleotides are commonly used in the food, feed, agriculture, medicine, and light industries [15–17]. At present, the main industrial RNA-producing species are the ascomycete budding yeasts *Saccharomyces cerevisiae* and *Candida tropicalis* (*C. tropicalis*) [18–20]. Fermentation kinetic models are an important technology for the study of microbial growth, substrate utilization, and product formation. Recently, these models have been the focus of research in bioprocessing [21–23]. It has been proposed that unstructured kinetic models can be fitted to describe the principal kinetics involved in ethanol fermentation in a continuous and closed-loop fermentation process with a pervaporation membrane bioreactor, and the models showed good agreement with the experimental data [24]. Unstructured kinetic models in a 50 L airlift bioreactor have been constructed for batch RNA production utilizing the Logistic–Monod model for microbial growth, the Luedeking–Piret model for product formation, and the modified Luedeking–Piret model for substrate uptake [19]. However, fermentation kinetic models of high-oxygen-consuming fermentation processes are rarely reported in airlift bioreactors with a high volumetric gas–liquid mass transfer coefficient.

In this study, a strain of *C. tropicalis* that produces large amounts of RNA was used as the producing strain, molasses and glucose served as the carbon sources, and unstructured kinetic models were built to analyze the fermentation process. The volumetric oxygen mass transfer coefficients (k_La) in batch and continuous fermentation for RNA production in a conventional cylinder airlift bioreactor (CCAB) and a rectangular dynamic membrane airlift bioreactor (RDMAB) were compared. Our study provides a theoretical basis for industrial production using fermentation processes in a dynamic membrane airlift bioreactor.

2. Rectangular dynamic membrane airlift bioreactor

The k_La value is predominantly determined by the total gas–liquid interfacial area (a) and the liquid mass transfer coefficient (k_L). The value of a is mainly related to the bubble size and gas holdup in the bioreactor [9]. Fine bubbles have a higher k_La than coarse bubbles with the same gas holdup because of the high total gas–liquid interfacial area. The size of the bubbles generated by dynamic membranes is affected by the relative liquid velocity, gas–liquid transmembrane pressure differences, liquid viscosity, and surface tension [25–27]. The higher the relative velocity of the liquid in the membrane pore surface, the smaller the bubble size. The liquid relative velocity on the surface of the dynamic membrane is increased by high speed rotation, which reduces the size of the bubbles [28]. Dynamic membranes exhibit increased k_La and improved gas holdup because they form an abundance of uniform fine bubbles [9]. In the present study, a dynamic membrane was used as the aeration unit in the airlift bioreactor (Fig. 1). As shown in Fig. 1(b), the dynamic membrane had a hollow structure, and the blades were made of a metal membrane with a pore size of 500 nm. Air enters through the air inlet, passes through the hollow shaft, and enters the dynamic membrane hollow area. Subsequently, because of the transmembrane pressure difference, air enters the fluid through the nanopores, forming fine bubbles.

Rectangular airlift bioreactors have improved mixing and mass transfer performance than those of cylinder airlift bioreactors because of the effects of their geometrical and operating parameters on hydrodynamics and mass transfer [29–31]. It has been reported that the hydrodynamic characteristics of a rectangular airlift loop reactor are better for gas holdup and the mass transfer coefficient than those of the cylinder airlift loop reactor [32]. The average k_La of the rectangular airlift loop reactor is approximately 40% greater than that of the cylinder airlift loop reactor [32]. The pre-experiment results showed that the gas holdup and mass transfer characteristics of the rectangular airlift reactor are better than those of the circular airlift reactor, which is consistent with many reported results [31,32]. Therefore, a new rectangular airlift bioreactor coupled with a dynamic membrane was developed, and schematic diagrams of the RDMAB and CCAB are shown in Fig. 1. The air circulation and schematic diagram of the double-layer dynamic membrane in the RDMAB is shown in Fig. 1(c). A double-layer dynamic membrane with a pore size of 500 nm was adopted to ensure almost the same air flux and to control the bubble diameter. Based on the optimization, the dynamic membrane was located at the lowest position inside the draft tube. An air compressor was used to supply air. Table 1 shows the detailed structural dimensions of the RDMAB and CCAB. Both the CCAB as a control and the RDMAB had volumes of 120 L. The volume of the liquid was 100 L. A transparent square glass cell was assembled outside the tank to observe the bubbles.

3. Materials and methods

3.1. Measurement of the volumetric oxygen mass transfer coefficient

The volumetric oxygen mass transfer coefficient (k_La) was determined using a dissolved oxygen (DO) probe (Mettler-Toledo, USA) with a response time of 15 s in the riser and downcomer pipes of the CCAB and RDMAB [9]. Two DO probes were installed in the riser at 0.300 m (position 14) and in the downcomer at 0.200 m (position 8) sections from the lower edge of the rectangular draft tube. The k_La values in the riser and downcomer were measured simultaneously. Briefly, nitrogen was bubbled into distilled water until the DO concentration reached less than 5% oxygen saturation. The nitrogen flow was then interrupted, nitrogen bubbles were released, and air was bubbled into the solution. The increase in the DO concentration was monitored over time until it reached 90% oxygen saturation. All experiments were conducted in triplicate. k_La was calculated using Eqs. (1) and (2):

$$\frac{dc_p}{dt} = \frac{c - c_p}{\tau_t} \tag{1}$$

$$\frac{dc}{dt} = k_La(c^* - c) \tag{2}$$

where c_p is the measured DO concentration in the liquid phase ($mol \cdot L^{-1}$), c is the actual DO concentration ($mol \cdot L^{-1}$), t is the fermentation time (s), c^* is the saturated DO concentration ($mol \cdot L^{-1}$), τ_t is the probe response time (s), and k_La is the volumetric oxygen mass transfer coefficient (s^{-1}).

3.2. Measurement of the gas holdup

The overall gas holdup was calculated by measuring the liquid level before and after aeration. All experiments were performed in triplicate. The overall gas holdup ε_T was calculated using Eq. (3):

$$\varepsilon_T = \frac{h_G - h_L}{h_L} \tag{3}$$

where h_L is the liquid level before aeration (m), and h_G is the liquid level during aeration (m).

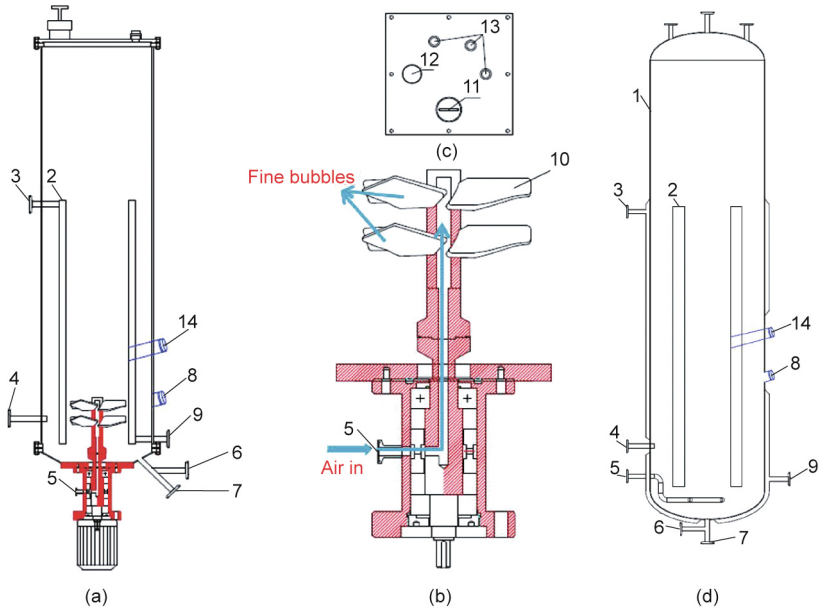

Fig. 1. (a) Schematic diagram of the rectangular dynamic membrane airlift bioreactor, (b) the dynamic membrane, (c) the rectangular cover, and (d) the conventional cylinder airlift bioreactor. (1: Bioreactor tank; 2: draft tube; 3: steam inlet or cooling water outlet; 4: sampling outlet; 5: air inlet; 6: continuous fermentation inlet; 7: continuous fermentation outlet; 8: thermometer, pH meter, and dissolved oxygen meter (DO) in downcomer; 9: condensate water outlet or cooling water inlet; 10: dynamic membrane blade; 11: inoculation inlet; 12: tail gas outlet; 13: feeding inlet, and 14: DO meter in riser).

Table 1
Structure dimensions of the RDMAB and the CCAB.

Dimension	Value	
	RDMAB	CCAB
Tank height (m)	1.200	1.200
Tank inner diameter or width (m)	0.320	0.360
Draft tube height (m)	0.660	0.660
Draft tube inner diameter or width (m)	0.220	0.240
Draft tube outer diameter or width (m)	0.230	0.250
Cross-sectional area ratio of downcomer to riser	1.023	1.165

3.3. Measurement of the bubble size

The bubble size distribution was measured by high-speed microscopic photography (Phantom VEO 1310; Vision Research, Inc., USA) equipped with a Nikon 105 mm F/2.8 micro lens (Nikon, Japan) to produce a controllable field-of-view down to a few millimeters. The images were processed manually by measuring the diameter of approximately 500 randomly selected bubbles.

3.4. Microorganism and culture conditions

The *C. tropicalis* strain NY6-18, which was used for RNA production in this study, was stored in our laboratory at −80 °C in 20% (v/v) glycerol. Molasses containing glucose with 50% mass fraction was used. The strain was cultured on a solid agar plate containing 20 g·L^{-1} glucose, 20 g·L^{-1} peptone, 10 g·L^{-1} yeast extract, and 20 g·L^{-1} agar for 72 h at 33 °C, after which it was stored at 4 °C.

The primary seed medium consisted of 21 g·L^{-1} glucose, 9 g·L^{-1} molasses, 10 g·L^{-1} $(NH_4)_2SO_4$, 0.5 g·L^{-1} $MgSO_4$, 3 g·L^{-1} H_3PO_4, 0.05 g·L^{-1} $ZnSO_4$, and 0.05 g·L^{-1} $FeSO_4$. The pH was adjusted to 4.0 with 25% aqueous ammonia, and the medium was sterilized for 15 min at 12 °C in an autoclave (YXQ-LS-75S11; Shanghai Boxun Medical Biological Instrument Corp., China).

The secondary seed medium consisted of 28 g·L^{-1} glucose, 12 g·L^{-1} molasses, 10 g·L^{-1} $(NH_4)_2SO_4$, 0.5 g·L^{-1} $MgSO_4$, 3 g·L^{-1} H_3PO_4, 0.05 g·L^{-1} $ZnSO_4$, and 0.05 g·L^{-1} $FeSO_4$. The medium was adjusted to pH 4.0 with 25% aqueous ammonia and sterilized for 15 min at 121 °C in an autoclave.

The fermentation medium consisted of 210 g·L^{-1} glucose, 90 g·L^{-1} molasses, 100 g·L^{-1} $(NH_4)_2SO_4$, 5 g·L^{-1} $MgSO_4$, 30 g·L^{-1} H_3PO_4, 0.5 g·L^{-1} $ZnSO_4$, and 0.5 g·L^{-1} $FeSO_4$. The pH of the medium was adjusted to 2.0 using 25% aqueous ammonia.

For seed culture, the strain was transferred from a solid agar plate into an Erlenmeyer flask (500 mL) containing 50 mL of the primary seed medium. The strain was cultured at 33 °C with shaking at 150 r·min^{-1} in a thermostatic incubator (HNY-211B; Tianjin Ounuo Instrument Corp., China) for 18 h. The primary inoculum (10%, v/v) was then transferred to a 15 L airlift bioreactor (Huike Bioengineering, China) containing 9 L of the secondary seed medium. The temperature was controlled at 33 °C, and the pH was maintained at 4.0 by the addition of aqueous ammonia. The aeration rate during incubation was 2.5 volume (air)/volume (culture) per minute (vvm), and peanut oil was used as an antifoam agent. Finally, the secondary inoculum (10%, v/v) was transferred into a 120 L CCAB (Huike Bioengineering) or RDMAB (constructed in our laboratory) containing 80 L of fermentation medium that had been sterilized for 15 min at 121 °C in an autoclave. The temperature was controlled at 33 °C, and the pH was maintained at 4.0 by adding aqueous ammonia. The aeration rate during incubation was 3.0 vvm and the dynamic membrane speed in the RDMAB was 400 r·min^{-1}. Continuous fermentation conditions were controlled to be the same as those used for batch fermentation. Bioreactor operation was initially conducted in batch fermentation mode until a significant amount of biomass was produced, after which additional fermentation medium (unsterilized) was added to the airlift bioreactor operated in continuous fermentation mode. All experiments were conducted in triplicate.

3.5. Biomass and glucose determination

Samples (5 mL) of the fermentation broth were transferred to dry, weighed centrifuge tubes, which were centrifuged for 15 min at 8000 r·min^{-1}. The mycelial pellets were washed three times with deionized water, after which the mycelium was dried

in an oven at 80 °C and weighed, and the biomass (dry cell weight, DCW) was calculated using Eq. (4):

$$\mathrm{DCW} = \frac{w}{v} \tag{4}$$

where DCW is the dry cell weight or biomass ($g{\cdot}L^{-1}$), w is the weight of the mycelium (g), and v is the volume of the fermentation broth (L).

Glucose concentration was determined using an automated enzyme analysis system (SBA-40C; Biology Institute of Shandong Academy of Sciences, China).

3.6. RNA assay

Two replicate 2 mL samples of fermentation broth were placed in 5 mL centrifuge tubes and centrifuged at 8000 $r{\cdot}min^{-1}$ for 15 min. The mycelial pellets were washed three times with deionized water, and one centrifuge tube was dried and weighed in an oven at 80 °C. Precooled 0.25 $mol{\cdot}L^{-1}$ perchloric acid solution (2 mL) was added to another centrifuge tube, which was shaken well and heated in a 70 °C water bath for 20 min, cooled in an ice bath to 25 °C, and centrifuged at 8000 $r{\cdot}min^{-1}$ for 10 min. Subsequently, a 1 mL sample of the supernatant was placed into a 100 mL volumetric flask and the volume was adjusted to 100 mL with deionized water. The absorption value was measured at a wavelength of 260 nm, and deionized water was used as a blank. The formula for determining the RNA concentration was as follows:

$$\text{RNA concentration} = \frac{A \times N \times 2}{M \times 26} \times 100\% \tag{5}$$

where A is the absorbance value of the sample solution, N is the dilution factor of the sample, 2 is the volume of 0.25 $mol{\cdot}L^{-1}$ perchloric acid (mL), M is the dry cell weight of mycelium in 2 mL of fermentation broth (mg), and 26 is the absorbance value of RNA.

3.7. Kinetic models

High substrate concentrations can result in substrate inhibition. To accurately describe the microbial growth kinetics with both substrate-limiting and self-inhibiting factors, a hybrid Logistic–Monod model has been used to analyze microbial growth in the batch fermentation process [33,34]. In our study, a hybrid Logistic–Monod model was used to fit the growth of *C. tropicalis* using Eq. (6):

$$\frac{\mathrm{d}X}{\mathrm{d}t} = \mu_{\max}\frac{S}{K_s + S}\left[1 - \frac{X}{X_{\max}}\right] \tag{6}$$

where X is the biomass concentration ($g{\cdot}L^{-1}$), t is the fermentation time (s), $\mu_{\max}$ is the maximum specific growth rate (h^{-1}), $X_{\max}$ is the maximum value of the biomass concentration ($g{\cdot}L^{-1}$), S is the substrate concentration ($g{\cdot}L^{-1}$), and K_s is the saturation coefficient ($g{\cdot}L^{-1}$).

The Luedeking–Piret model is often used to explain the synthesis of metabolites by combining both growth- and non-growth-associated contributions [35,36]. Therefore, RNA production can be described by the Luedeking–Piret model using Eq. (7):

$$\frac{\mathrm{d}P}{\mathrm{d}t} = \alpha\frac{\mathrm{d}X}{\mathrm{d}t} + \beta X \tag{7}$$

where P is the RNA concentration ($g{\cdot}L^{-1}$), α is the growth correlation coefficient ($g{\cdot}g^{-1}$), and β is the non-growth correlation coefficient ($g{\cdot}L^{-1}{\cdot}h^{-1}$).

The substrate utilization rate in the fermentation broth is related to the biomass and product formation rate. There are three aspects to substrate consumption: ① providing energy and nutrients for cell growth, ② maintaining cell activity, and ③ promoting product formation. A modified Luedeking–Piret model can be used to describe the relationship between substrate utilization and product production, including substrate consumption for maintaining cell growth and substrate transformation [37,38]. Therefore, a modified Luedeking–Piret model was employed to explain substrate utilization in *C. tropicalis* using Eq. (8):

$$-\frac{\mathrm{d}S}{\mathrm{d}t} = \frac{1}{Y_{X/S}}\frac{\mathrm{d}X}{\mathrm{d}t} + \frac{1}{Y_{P/S}}\frac{\mathrm{d}P}{\mathrm{d}t} + mX \tag{8}$$

where m is the cell maintenance correlation coefficient ($g{\cdot}g^{-1}{\cdot}h^{-1}$), $Y_{X/S}$ is the yield coefficient of biomass on the substrate ($g{\cdot}g^{-1}$), and $Y_{P/S}$ is the yield coefficient of RNA on the substrate ($g{\cdot}g^{-1}$).

4. Results and discussion

4.1. Volumetric oxygen mass transfer coefficient

The k_La value is a key indicator for evaluating bioreactor performance. The k_La values of the riser and downcomer pipes of the CCAB and RDMAB operating at 0, 200, and 400 $r{\cdot}min^{-1}$ were compared and are shown in Fig. 2. The RDMAB operating at 0, 200, and 400 $r{\cdot}min^{-1}$ showed higher k_La values than those with the CCAB. The air aeration rate increased continuously, and the value of k_La increased. When the air aeration rate increased to 0.3 $m^3{\cdot}min^{-1}$, which is equivalent to 3.0 vvm, the k_La values of the riser in the RDMAB operating at 0, 200, and 400 $r{\cdot}min^{-1}$ were 0.091, 0.097, and 0.112 s^{-1}, respectively, while the k_La value of the riser in the CCAB was only 0.07 s^{-1}. As the speed increased, the proportion of fine bubbles increased and the bubble size decreased continuously; the k_La value also increased continuously, which is consistent with previously reported results [9]. The dynamic membrane generates a large number of fine bubbles, which increases the oxygen mass transfer in the airlift bioreactor.

4.2. Gas holdup

The overall gas holdup was determined in an air–water system for CCAB and RDMAB operating at speeds of 0, 200, and 400 $r{\cdot}min^{-1}$. As shown in Fig. 3, increased aeration levels from 0.5 to 3.0 vvm resulted in elevated overall gas holdup levels in both the CCAB and RDMAB operating at speeds of 0, 200, and 400 $r{\cdot}min^{-1}$. In the RDMAB operating at speeds of 0, 200, and 400 $r{\cdot}min^{-1}$, the overall gas holdups were higher than those in the CCAB system under the same conditions. Compared with coarse bubbles, fine bubbles have a lower velocity and longer residence time, which is beneficial for increasing the overall gas holdup [9].

4.3. Bubble size

Fig. 4 shows the bubble size distributions and shapes in the RDMAB operating at a speed of 200 $r{\cdot}min^{-1}$ at aeration rates of 0.5, 1.0, 1.5, and 2.0 vvm. The diameter of the bubbles produced by low aeration was small, and the bubble shape in the RDMAB tended to be spherical. The bubble size was evenly distributed and concentrated in a narrow range in the RDMAB when aeration was less than 2.0 vvm. The size distributions of the bubbles in the RDMAB are shown in Fig. 5. The Sauter mean diameter (d_{32}) of the bubbles in the RDMAB at aerations of 0.5, 1.0, 1.5, 2.0, 2.5, and 3.0 vvm were (0.89 ± 0.40), (0.94 ± 0.47), (1.10 ± 0.54), (1.19 ± 0.72), (1.22 ± 0.90), and (1.25 ± 0.94) mm, respectively, which were obviously smaller than those reported for airlift reactors [39]. It was also found that the bubble diameter increased with increasing aeration. The Sauter mean diameter of the bubbles in the RDMAB at speeds of 0, 200, and 400 $r{\cdot}min^{-1}$ were (0.97 ± 0.36),

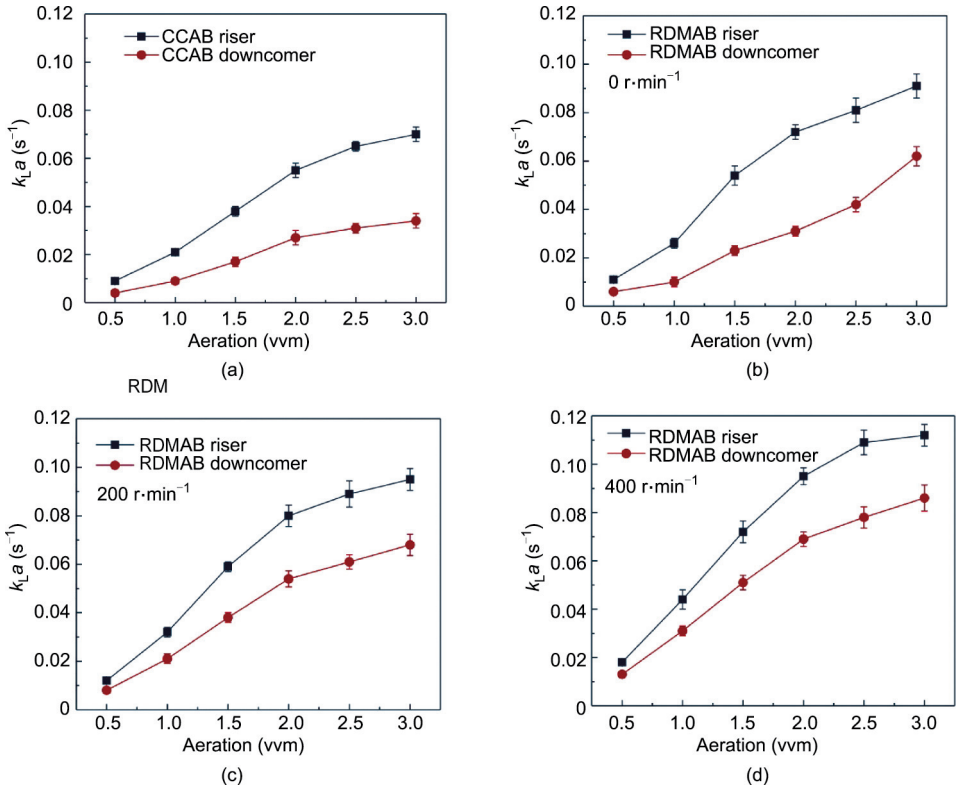

Fig. 2. Comparison of k_La of the riser and downcomer of (a) the CCAB and (b)–(d) the RDMAB operating at speeds of 0, 200, and 400 r·min^{-1}, respectively.

(0.95 ± 0.43), and (0.93 ± 0.39) mm, respectively, which indicates that speed has little effect on the bubble diameter. The main parameter of gas–liquid mass transfer is aeration, and the rotation can enhance the gas–liquid mass transfer by improving the gas–liquid mixing efficiency.

4.4. Comparison of present data with published results

A variety of data on the hydrodynamics and mass transfer of airlift reactors for Newtonian fluids can be found in the literature. A comparison of our data with literature data is shown in Table 2 [39–44]. Compared with conventional internal loop airlift reactors, many modified airlift reactors with mass transfer intensification have higher k_La values. Rectangular airlift reactors such as RDMAB and split-rectangle-internal loop airlift bioreactors show higher k_La values than those of conventional circular airlift reactors, even at low aeration levels [43]. The key reason for this phenomenon is that a rectangular structure has a better flow field to promote gas–liquid mass transfer [43]. In addition, a variety of mass transfer intensification methods can significantly enhance gas–liquid mass transfer, such as net draft tubes and helical sieve plates [39,40]. Helical sieve plates cut large bubbles into small bubbles with an enhanced gas–liquid mass transfer rate. As mentioned above, a rectangular dynamic membrane airlift bioreactor has extraordinary advantages and development potential in biological fermentation processes.

4.5. Batch fermentation in the CCAB and RDMAB

The biomass concentration, RNA concentration, sugar concentration, and DO level for *C. tropicalis* cultured in the CCAB and RDMAB were obtained in batch fermentation mode, and the results are shown in Fig. 6. During batch fermentation, the biomass level and RNA concentration in the RDMAB were higher than those in the CCAB, which indicates that biomass growth and product synthesis were promoted in the RDMAB because of an adequate oxygen supply. The RNA concentration in the fermentation broth seems to parallel microbial growth in CCAB and RDMAB. The biomass and RNA concentrations increased constantly, while the sugar concentration decreased constantly. The rate of sugar consumption in the RDMAB was significantly higher than that in the CCAB, which demonstrates that sugar was more efficiently converted into both products and biomass. A high DO level can promote product accumulation in a high-oxygen-consumption and high-density fermentation process. Variation in the DO level affects biomass concentration, lipid accumulation, and composition [45].

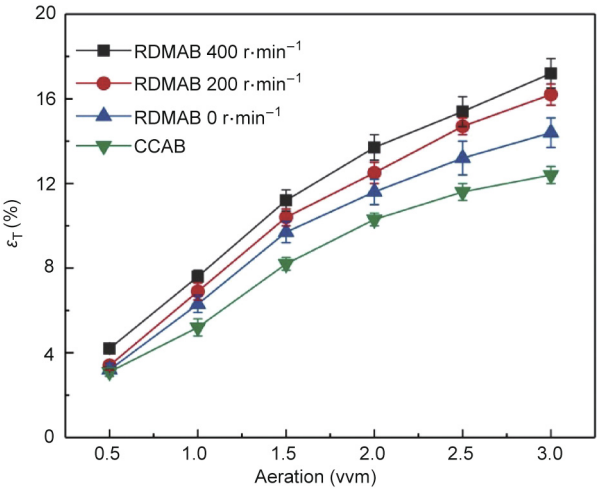

Fig. 3. Comparison of overall gas holdup the CCAB and the RDMAB operating at speeds of 0, 200, and 400 r·min^{-1} at different aeration.

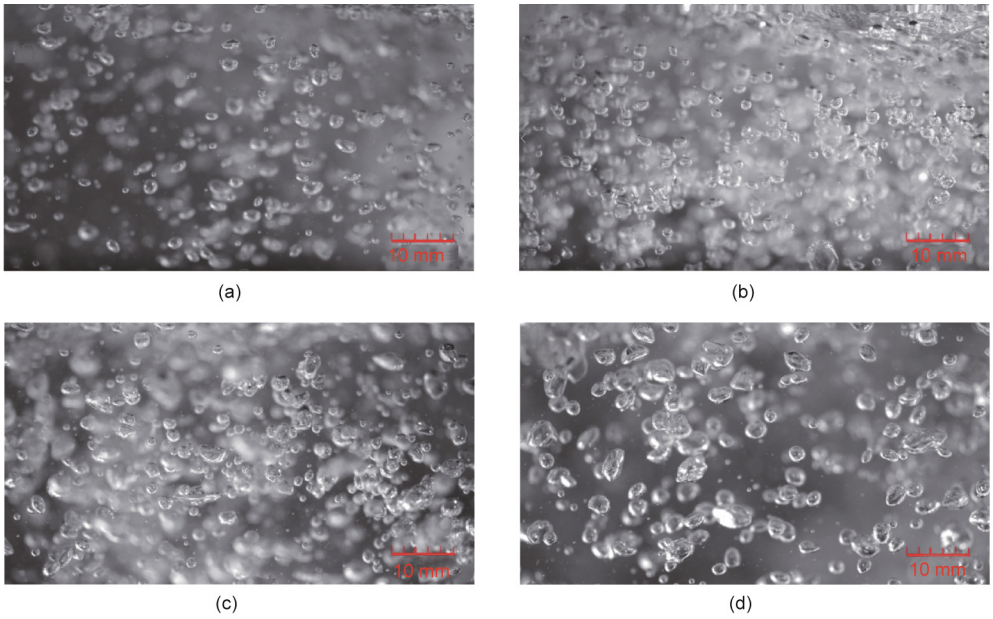

Fig. 4. Bubble size distributions and shapes in the RDMAB operating at speed of 200 r·min^{-1} at aeration of (a) 0.5, (b) 1.0, (c) 1.5, and (d) 2.0 vvm.

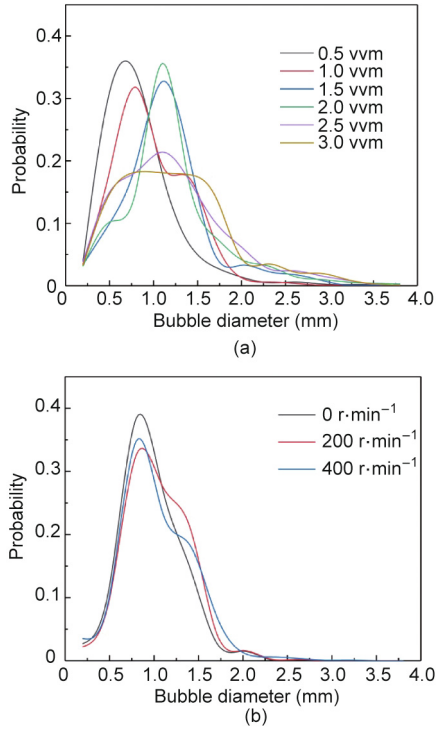

Fig. 5. Size distribution of bubbles in RDMAB operating at (a) aeration of 0.5–3.0 vvm when speed of 200 r·min^{-1} and (b) speeds of 0, 200, and 400 r·min^{-1} when aeration of 1.0 vvm.

High RNA production by *C. tropicalis* is a high-oxygen-consumption bioprocess. RDMAB provides a high DO level or k_La to improve RNA accumulation. Finally, the maximum RNA concentration and biomass production in the RDMAB after 120 h of fermentation were 14.10 and 84.02 g·L^{-1} respectively, which were much higher than those attained in the CCAB at 13.0 and 73.5 g·L^{-1}, respectively.

The starting time of continuous fermentation is very important to continuously and efficiently produce fermentation products, and the starting time of continuous fermentation can be determined by the microbial growth curve in batch fermentation mode. In general, different bioreactors may have different optimal starting times for continuous fermentation. Under batch fermentation conditions, the oxygen uptake rate increases rapidly, and the biomass level reaches 40%–80% of the maximum. This point in time can be considered as the starting time for continuous fermentation [46]. Fig. 6(a) shows that, in the CCAB, the oxygen uptake rate was the highest and the DO level reached the lowest point at 70 h of fermentation time, and the biomass level reached 68.4% of maximum. Therefore, 70 h was chosen as the starting time for continuous fermentation in the CCAB. Fig. 6(b) shows that in the RDMAB, the oxygen uptake rate was the highest and the DO was the lowest at 50 h of fermentation, and the DCW (biomass) reached 71.4% of maximum. Therefore, 50 h was chosen as the starting time for continuous fermentation in the RDMAB. Figs. 6(a) and (b) shows that the starting time for continuous fermentation in the RDMAB was 20 h earlier than that in the CCAB. The k_La in the RDMAB was higher than that in the CCAB, and the microorganism (*C. tropicalis*) had a higher biological activity, faster growth rate, and slower senescence rate under growth conditions with a sufficient supply of oxygen.

4.6. Kinetic models of batch fermentation in the CCAB and RDMAB

The fitting curves for biomass concentration, RNA concentration, and sugar concentration during batch fermentation in the CCAB and RDMAB are shown in Fig. 7. The Logistic–Monod, Luedeking–Piret, and modified Luedeking–Piret parameters are summarized in Table 3. The correlation coefficients (R^2) of microbial growth in the CCAB and RDMAB were 0.9496 and 0.9527, respectively (Fig. 7(a)). Our results show that the experimental data agreed well with the prediction model. The microbial growth curves in the CCAB and RDMAB are typical sigmoidal curves. The growth curves can be structured as a lag phase, exponential growth phase, decelerating growth phase, and stationary phase [19,47]. In addition, we found that the X_{max}, K_s, and μ_{max} in the RDMAB were 81.04 g·L^{-1}, 5.097 g·L^{-1}, and 0.10680 h^{-1} respectively, considerably higher than those in the CCAB (74.55 g·L^{-1}, 2.954 g·L^{-1}, and 0.07061 h^{-1}, respectively), which shows that a high k_La can significantly increase the growth of microorganisms and avoid

Table 2
Comparison of present data with published results.

Airlift reactors	Sparger	Medium	Aeration (vvm)	ε_T (%)	k_La (s^{-1})	Reference
Rectangular airlift bioreactor	Dynamic membrane	Water	0.5–3.0	3.2–17.2	0.010–0.112	This work
Airlift reactor with helical sieve plates	Steel pipe with holes	Water	0.6–6.0	1.0–15.0	0.010–0.135	[39]
Airlift reactor with a net draft tube	Perforated	Water	0.25–2.5	1.0–5.8	0.005–0.031	[40]
Airlift bioreactor with helical sieve plates	Conical	Water	0.33–2.0	1.3–11.0	0.007–0.090	[41]
Center-rising airlift reactor	Perforated	Water	0.167–1.0	0.8–4.2	0.0035–0.0190	[42]
Annulus-rising airlift reactor	O-ring	Water	0.167–1.0	0.8–4.8	0.0035–0.0200	[42]
Split-rectangle-internal loop airlift bioreactor	Perforated	Water	0.4–1.2	11.2–21.3	0.065–0.118	[43]
Airlift reactor	Orifice	Water	0.1–1.5	1.0–8.9	0.002–0.010	[44]

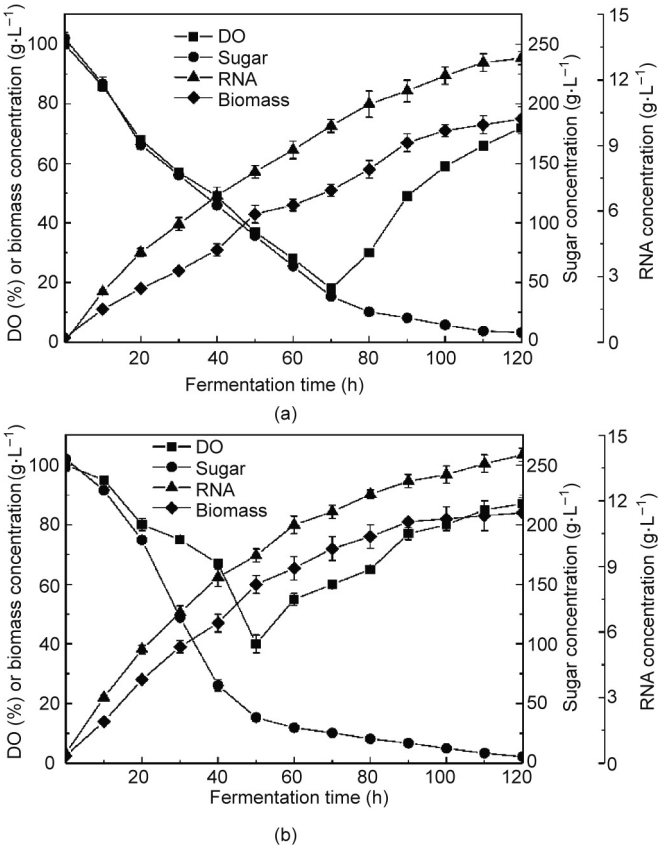

Fig. 6. Batch fermentation for RNA production in (a) the CCAB and (b) the RDMAB.

the limitation of hypoxia. In the initial stage of fermentation, the substrate concentration is much higher than the saturation coefficient, which indicates that microbial growth is not limited by the substrate concentration. When the sugar concentration is less than 50 $g{\cdot}L^{-1}$, microbial growth can be restricted by the low sugar concentration. At this time, feeding is required to promote microbial growth. As shown in Fig. 6, we found that when the fermentation time was 50 h (the starting time of continuous fermentation in the RDMAB, the sugar concentration in the RDMAB was < 50 $g{\cdot}L^{-1}$, and the fermentation time in the CCAB was 70 h (the starting time of continuous fermentation in the CCAB).

The Luedeking–Piret model fitted to the RNA production is shown in Fig. 7(b). The correlation coefficients (R^2) for RNA concentration in the CCAB and RDMAB were 0.9553 and 0.9679, respectively. Our results show that the experimental data agreed well with the prediction model. The Luedeking–Piret parameters α and β are classified into three categories: ① $\alpha \neq 0$ and $\beta = 0$, product formation is growth-associated; ② $\alpha = 0$ and $\beta \neq 0$, product formation is non-growth-associated; and ③ $\alpha \neq 0$ and $\beta \neq 0$, product formation is mixed-growth-associated [34]. In this study, the growth correlation coefficients (α) in the CCAB and RDMAB were 0.1206 and 0.1035 $g{\cdot}g^{-1}$, respectively, and the non-growth correlation coefficients (β) were 0.0004057 and 0.0005286 $g{\cdot}L^{-1}{\cdot}h^{-1}$, respectively, which showed that the Luedeking–Piret model of RNA production belonged to a mixed-growth-associated pattern (category #3). The RNA concentration increased almost proportionally with the increase in biomass during fermentation. The value of α in the RDMAB was lower than that in the CCAB, which indicates that the conversion efficiency of substrate sugars into the product was higher in the RDMAB.

Substrate utilization is related to microbial growth, RNA production, and substrate uptake, which are required for cell maintenance. In the fermentation process, sugars are used as carbon sources, and a kinetic model of sugar utilization was established using the modified Luedeking–Piret model, as shown in Fig. 7(c). The correlation coefficients (R^2) of the model for the CCAB and RDMAB were 0.9834 and 0.9732, respectively, which indicates that the model fitted to the experimental data satisfactorily. The yield coefficients of biomass on the substrate ($Y_{X/S}$) in the CCAB and RDMAB were 0.8178 and 0.4686 $g{\cdot}g^{-1}$, respectively, and the yield coefficients of RNA on the substrate ($Y_{P/S}$) were 0.04127 and 0.09196 $g{\cdot}g^{-1}$, respectively, indicating that sufficient oxygen levels are more favorable for the conversion of substrate sugars into RNA production. k_La is a key fermentation parameter for producing highly aerobic products. Compared with those in the CCAB, the dynamic membrane in the RDMAB can produce higher k_La values [9]. Chang et al. [48] found that a high k_La could effectively increase the docosahexaenoic acid concentration, docosahexaenoic acid productivity, and conversion yield, which is consistent with the results of our study.

The models were validated by changing the initial sugar concentration (200 $g{\cdot}L^{-1}$) of the medium. The results of the Logistic–Monod model fitted to microbial growth, Luedeking–Piret model fitted to RNA production, and modified Luedeking–Piret model fitted to substrate utilization were more than 90% accurate, which indicates that the models are reliable and robust.

4.7. Continuous fermentation in the CCAB and RDMAB

Continuous fermentation, based on batch fermentation, needs to meet the following assumptions: ① The bioreactors are in the chemostat culture state in the continuous fermentation process; ② the physiological state of each stage in the bioreactor is maintained in the continuous fermentation process in the chemostat; and ③ the parameters of continuous fermentation, such as microbial growth, product formation, and substrate consumption, are in good agreement with those of batch fermentation [33,49]. Therefore, the initial dilution rate for continuous fermentation was obtained using the batch fermentation kinetic model.

The dilution rate was the feed flow rate divided by the culture volume. In the continuous fermentation mode, the specific growth rate (μ) is related to the dilution rate (D_r) in the mass balance model [50]:

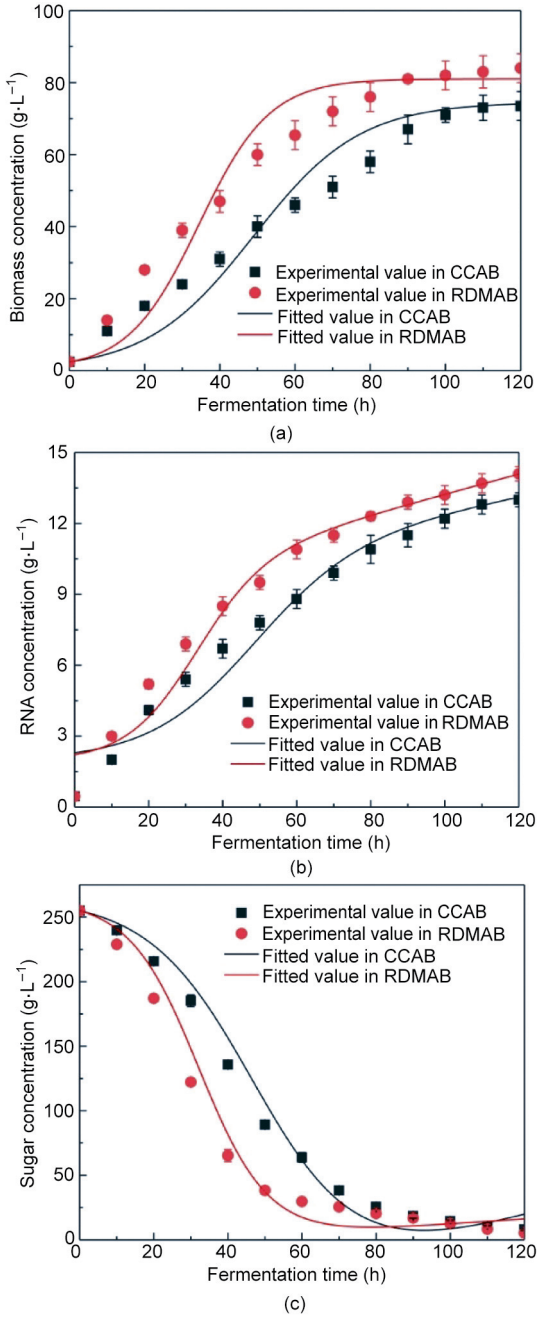

Fig. 7. Model fitting curves of (a) biomass in the CCAB (R^2 = 0.9496) and the RDMAB (R^2 = 0.9527); (b) RNA production in the CCAB (R^2 = 0.9553) and the RDMAB (R^2 = 0.9679); and (c) sugar concentration in the CCAB (R^2 = 0.9834) and the RDMAB (R^2 = 0.9732).

$$(\mu - D_r)X = \frac{dX}{dt} \tag{9}$$

where D_r is the dilution rate (h^{-1}) and μ is the specific growth rate (h^{-1}).

At the steady state, $\mu = D_r$; thus, the initial dilution rate can be determined by the specific growth rate. In addition, D_r should not exceed μ_{max} to prevent washout.

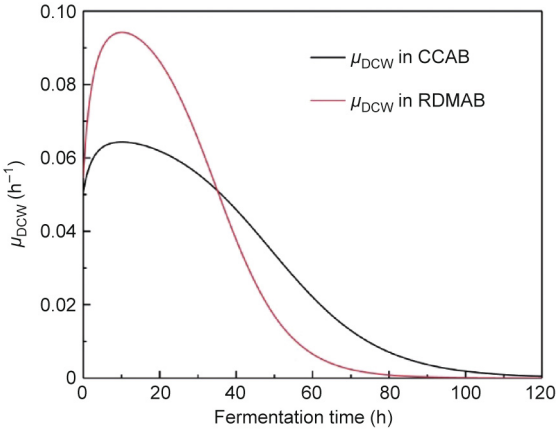

Fig. 8. Specific growth rates (μ_{DCW}) of *C. tropicalis* in the CCAB and the RDMAB.

The specific growth rates of microbial biomass in the batch fermentation mode in the CCAB and RDMAB are shown in Fig. 8. In the initial stage of fermentation, the specific growth rate in the RDMAB was significantly higher than that in the CCAB because of sufficient oxygen and substrate levels. With the rapid consumption of the substrate, the specific growth rates in both the CCAB and RDMAB decreased significantly. By comparing the maximal growth rate reported, the maximal growth rates in the RDMAB and CCAB in this study were lower than those previously reported due to high substrate concentrations. However, the average growth rate was consistent with previously reported results [19]. The starting times for continuous fermentation in the CCAB and RDMAB were determined to be 70 and 50 h, respectively, based on batch fermentation. The initial dilution rates during continuous fermentation in the CCAB and RDMAB were 0.01297 and 0.01684 h^{-1}, respectively. The initial dilution rate during continuous fermentation in the RDMAB was higher than that in the CCAB, which shows that rapid substrate consumption promotes biomass increase and substrate accumulation in the RDMAB.

Due to the high oxygen demand for the growth, maintenance, and metabolism of *C. tropicalis*, a sufficient oxygen supply is required in the bioreactor. The dynamic membrane in the airlift bioreactor provides fine bubbles by combining membrane micropores and the dissipation energy produced by dynamic membrane rotation. The bubble size in dynamic membrane aeration can reach the micron level to increase the specific surface area of the bubbles, which significantly increases the k_La and provides sufficient DO for microbial culture. Fig. 9 shows the biomass concentration, aeration, RNA concentration, and sugar concentration at 20% DO in the bioreactor for the CCAB and RDMAB while maintaining a constant dilution rate. Biomass accumulation in the RDMAB was 9.71% higher than that in the CCAB, and the RNA concentration in the RDMAB was 11.15% higher than that in the CCAB. The yield of RNA (RNA production/sugar consumed) in the RDMAB was 0.069 g RNA per gram of sugar, which was 11.29% higher than that in the CCAB (0.062 g RNA per gram of sugar). The average productivity of RNA in the RDMAB was 0.117 g·L^{-1}·h^{-1}, which was 8.3% higher than that in the CCAB (0.108 g L^{-1}·h^{-1}). However, the air aeration of the CCAB was 59.4% higher than that of the RDMAB. If the CCAB and RDMAB need to provide a constant DO level, the

Table 3
Parameters of kinetic models.

Bioreactor	μ_{max} (h^{-1})	X_{max} (g·L^{-1})	K_S (g·L^{-1})	α (g·g^{-1})	β (g·L^{-1}·h^{-1})	$Y_{X/S}$ (g·g^{-1})	$Y_{P/S}$ (g·g^{-1})
CCAB	0.07061	74.55	2.954	0.1206	0.0004057	0.8178	0.04127
RDMAB	0.10680	81.04	5.097	0.1035	0.0005286	0.4686	0.09196

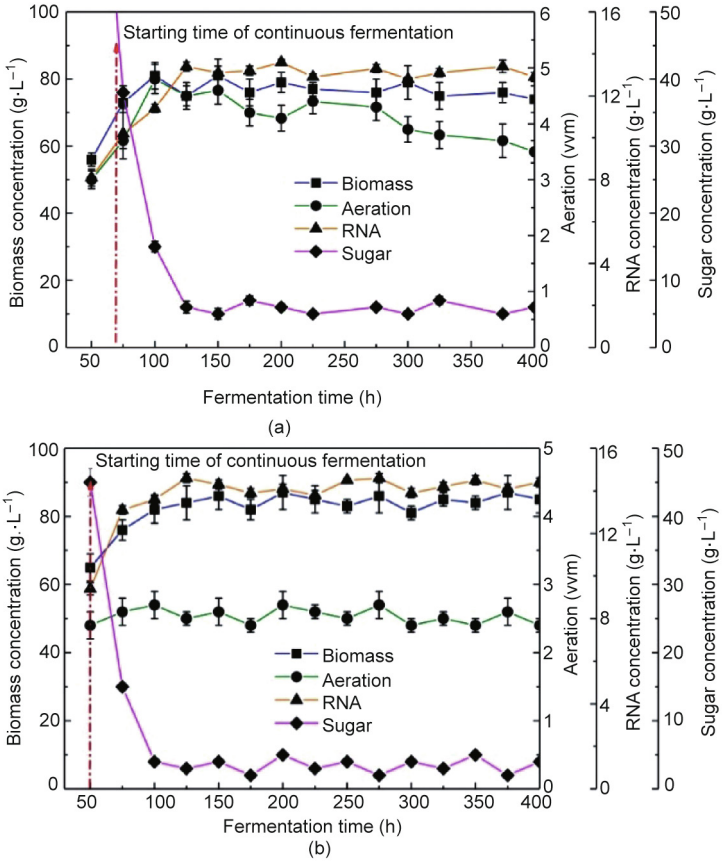

Fig. 9. Biomass, aeration, RNA concentration, and sugar concentration at 20% DO in (a) the CCAB and (b) the RDMAB.

CCAB must increase air aeration. However, with the increase in air aeration, bubbles break and coalesce in the solution, which may increase the shear stress and affect cell growth in the CCAB. The speed of the RDMAB was relatively similar to the reported speed of the stirred reactor [9]. The shear stress induced by stirring in the RDMAB had little adverse effect on the microorganism, which was confirmed by the RNA yield and biomass concentration. For aerobic fermentation, DO is not only a nutritional factor, but also an environmental factor. Compared with the perforated pipe on the CCAB, the rotation of the dynamic membrane in the RDMAB can increase the liquid velocity to promote gas–liquid mixing and further increase the k_La. The CO_2 level of the gas after fermentation in the RDMAB was 23.1% higher than that in the CCAB.

4.8. Dilution rate during continuous fermentation

In aerobic fermentation bioprocesses, the oxygen demands vary between different microbial strains and fermentation stages. The DO level in the fermentation broth can directly affect enzyme activity, metabolic pathways, and product yield in microorganisms. During the fermentation process, k_La is mainly affected by the concentration of DO in the fermentation broth and the transfer resistance [45,51]. Dynamic membranes enhance the gas–liquid mass transfer coefficient by producing fine bubbles and promoting gas–liquid mixing [9]. Therefore, it is important to study the effects of DO levels on fermentation to improve bioprocesses. The dilution rate is the key index for continuous fermentation. The dilution rate is directly proportional to the maximum specific growth rate, indicating that the higher the specific growth rate, the higher the dilution rate. As shown in Fig. 10, under the same air aeration (3.0 vvm), the DO in the CCAB was 76.9% lower than that in the RDMAB, which led to different dilution rates in the two airlift bioreactors in

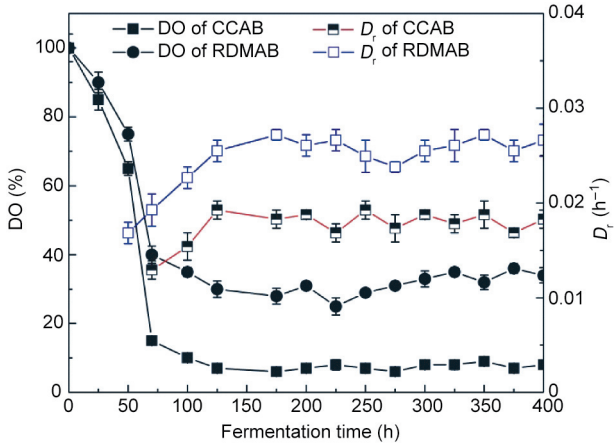

Fig. 10. DO level and dilution rate at the same aeration rate (3.0 vvm) in the CCAB and the RDMAB.

the continuous fermentation mode. The average dilution rate in the RDMAB was 39.6% higher than that in the CCAB. Therefore, the production capacity of the RDMAB in continuous fermentation mode may be greatly improved. Under the same air aeration (3.0 vvm), the RDMAB had a higher level of DO, which promoted the synthesis of the product.

5. Conclusions

In this study, we developed a novel RDMAB for producing fine bubbles to enhance the volumetric oxygen mass transfer

coefficient (k_La) and gas holdup, as well as improve the biological process in the bioreactor. In addition, unstructured kinetic models for microbial growth, substrate utilization, and RNA formation by *C. tropicalis* were established. During batch fermentation, the biomass, RNA yield, and substrate utilization in the RDMAB were higher than those in the CCAB. We found that the starting time of continuous fermentation in the RDMAB was 20 h earlier than that in the CCAB, which greatly improved the bioprocess. The biomass accumulation in the RDMAB was 9.71% higher than that in the CCAB, and the RNA production was 11.15% higher than that in the CCAB. Finally, the dilution rate in RDMAB was 39.6% higher than that in CCAB. To summarize, the RDMAB was superior to the CCAB in both batch and continuous fermentation modes. Improving the structure of the CCAB has far-reaching implications for bioprocessing, in addition to providing a reference for the improvement of other types of bioreactors.

Acknowledgments

This work was supported by National Key Research and Development Program of China (2020YFE0100100, 2021YFC2104100, and 2018YFA0901500), Basic Science (Natural Science) Research Project of Jiangsu Province Colleges and Universities (21KJB530014), and Jiangsu Synergetic Innovation Center for Advanced Bio-Manufacture.

Compliance with ethics guidelines

Ganlu Li, Kequan Chen, Yanpeng Wei, Jinlei Zeng, Yue Yang, Feng He, Hui Li, and Pingkai Ouyang declare that they have no conflict of interest or financial conflicts to disclose.

References

[1] Zhang T, We CH, Ren Y, Feng CH, Wu HZ. Advances in airlift reactors: modified design and optimization of operation conditions. Rev Chem Eng 2017;33(2):163–82.
[2] Särkelä R, Eerikäinen T, Pitkänen JP, Bankar S. Mixing efficiency studies in an airlift bioreactor with helical flow promoters for improved reactor performance. Chem Eng Process 2019;137:80–6.
[3] Yang T, Geng S, Yang C, Huang Q. Hydrodynamics and mass transfer in an internal airlift slurry reactor for process intensification. Chem Eng Sci 2018;184:126–33.
[4] Yen HW, Chang JT, Chang JS. The growth of oleaginous *Rhodotorula glutinis* in an internal-loop airlift bioreactor by using mixture substrates of rice straw hydrolysate and crude glycerol. Biomass Bioenergy 2015;80:38–43.
[5] Lin J, Han M, Wang T, Zhang T, Wang J, Jin Y. Influence of the gas distributor on the local hydrodynamic behavior of an external loop airlift reactor. Chem Eng J 2004;102(1):51–9.
[6] Chen Z, Min H, Hu D, Wang H, Zhao Y, Cui Y, et al. Performance of a novel multiple draft tubes airlift loop membrane bioreactor to treat ampicillin pharmaceutical wastewater under different temperatures. Chem Eng J 2020;380:122521.
[7] Medina-Moreno SA, Conde-Báez L, Jiménez-González A, Aguilar-López R, Rodríguez-Vázquez R, Tec-Caamal EN. Modelling hexadecane uptake strategies of a rhizospheric bacterial consortium under different hydrodynamic draft-tube airlift reactor conditions. Biochem Eng J 2020;160:107611.
[8] Manowattana A, Techapun C, Watanabe M, Chaiyaso T. Bioconversion of biodiesel-derived crude glycerol into lipids and carotenoids by an oleaginous red yeast *Sporidiobolus pararoseus* KM281507 in an airlift bioreactor. J Biosci Bioeng 2018;125(1):59–66.
[9] Li G, Li H, Wei G, He X, Xu S, Chen K, et al. Hydrodynamics, mass transfer and cell growth characteristics in a novel microbubble stirred bioreactor employing sintered porous metal plate impeller as gas sparger. Chem Eng Sci 2018;192:665–77.
[10] Imrat, Labala RK, Velhal S, Bhagat S, Patel V, Jeyaram K. Small double-stranded RNA with anti-HIV activity abundantly produced by *Bacillus subtilis* MTCC5480 isolated from fermented soybean. Int J Biol Macromol 2020;161:828–35.
[11] Bosco F, Casale A, Gribaudo G, Mollea C, Malucelli G. Nucleic acids from agro-industrial wastes: a green recovery method for fire retardant applications. Ind Crops Prod 2017;108:208–18.
[12] Tam TH, Chan KL, Boroumand P, Liu Z, Brozinick JT, Bui HH, et al. Nucleotides released from palmitate-activated murine macrophages attract neutrophils. J Biol Chem 2020;295(15):4902–11.
[13] Xu M, Liang R, Guo Q, Wang S, Zhao M, Zhang Z, et al. Dietary nucleotides extend the life span in Sprague-Dawley rats. J Nutr Health Aging 2013;17(3):223–9.
[14] Singhal A, Macfarlane G, Macfarlane S, Lanigan J, Kennedy K, Elias-Jones A, et al. Dietary nucleotides and fecal microbiota in formula-fed infants: a randomized controlled trial. Am J Clin Nutr 2008;87(6):1785–92.
[15] Del Arco J, Cejudo-Sanches J, Esteban I, Clemente-Suárez VJ, Hormigo D, Perona A, et al. Enzymatic production of dietary nucleotides from low-soluble purine bases by an efficient, thermostable and alkali-tolerant biocatalyst. Food Chem 2017;237:605–11.
[16] Sauer N, Eklund M, Hoerner S, Bauer E, Jezierny D, Mosenthin R. Short-term effect of dietary yeast nucleotide supplementation on total and diurnal variation of small intestinal enzyme activities in piglets. J Anim Sci 2012;90(Suppl 4):179–81.
[17] Cai X, Bao L, Wang N, Ren J, Chen Q, Xu M, et al. Dietary nucleotides protect against alcoholic liver injury by attenuating inflammation and regulating gut microbiota in rats. Food Funct 2016;7(6):2898–908.
[18] Khatun F, Kurata K, Chuwattanakul V, Sugiyama M, Kaneko Y, Harashima S. Increased transcription of RPL40A and RPL40B is important for the improvement of RNA production in *Saccharomyces cerevisiae*. J Biosci Bioeng 2013;116(4):423–32.
[19] Li B, Chen X, Ren H, Li L, Xiong J, Bai J, et al. Kinetic models of ribonucleic acid fermentation and continuous culture by *Candida tropicalis* no.121. Bioprocess Biosyst Eng 2012;35(3):415–22.
[20] Chuwattanakul V, Sugiyama M, Khatun F, Kurata K, Tomita I, Kaneko Y, et al. Increased transcription of NOP15, involved in ribosome biogenesis in *Saccharomyces cerevisiae*, enhances the production yield of RNA as a source of nucleotide seasoning. J Biosci Bioeng 2012;114(1):17–22.
[21] Bedade DK, Dev MJ, Singhal RS. Bioreactor studies on acrylamidase produced from *Cupriavidus oxalaticus* ICTDB921: production, kinetic modeling, and purification. Biochem Eng J 2019;149:107245.
[22] Bamaalabong PP, Asiedu NY, Neba FA, Addo A. Dynamic behavior, simulations, and kinetic analysis of two dimensional substrate–product inhibitions in batch fermentation processes. Ind Eng Chem Res 2020;59(21):9797–807.
[23] Almquist J, Cvijovic M, Hatzimanikatis V, Nielsen J, Jirstrand M. Kinetic models in industrial biotechnology—improving cell factory performance. Metab Eng 2014;24:38–60.
[24] Fan S, Chen S, Tang X, Xiao Z, Deng Q, Yao P, et al. Kinetic model of continuous ethanol fermentation in closed-circulating process with pervaporation membrane bioreactor by *Saccharomyces cerevisiae*. Bioresour Technol 2015;177:169–75.
[25] Tanaka S, Kastens S, Fujioka S, Schlüter M, Terasaka K. Mass transfer from freely rising microbubbles in aqueous solutions of surfactant or salt. Chem Eng J 2020;387:121246.
[26] Nock WJ, Serna-Maza A, Heaven S, Banks CJ. Evaluation of microporous hollow fibre membranes for mass transfer of H_2 into anaerobic digesters for biomethanization. J Chem Technol Biotechnol 2019;94(8):2693–701.
[27] Tirunehe G, Norddahl B. The influence of polymeric membrane gas spargers on hydrodynamics and mass transfer in bubble column bioreactors. Bioprocess Biosyst Eng 2016;39(4):613–26.
[28] Fujikawa S, Zhang R, Hayama S, Peng G. The control of micro-air-bubble generation by a rotational porous plate. Int J Multiph Flow 2003;29(8):1221–36.
[29] Kilonzo PM, Margaritis A, Bergougnou MA, Yu J, Ye Q. Effects of geometrical design on hydrodynamic and mass transfer characteristics of a rectangular-column airlift bioreactor. Biochem Eng J 2007;34(3):279–88.
[30] Atenas M, Clark M, Lazarova V. Holdup and liquid circulation velocity in a rectangular air-lift bioreactor. Ind Eng Chem Res 1999;38(3):944–9.
[31] Drandev S, Penev KI, Karamanev D. Study of the hydrodynamics and mass transfer in a rectangular air-lift bioreactor. Chem Eng Sci 2016;146:180–8.
[32] Lu X, Ding J, Wang Y, Shi J. Comparison of the hydrodynamics and mass transfer characteristics of a modified square airlift reactor with common airlift reactors. Chem Eng Sci 2000;55(12):2257–63.
[33] Xu P. Analytical solution for a hybrid Logistic–Monod cell growth model in batch and continuous stirred tank reactor culture. Biotechnol Bioeng 2020;117(3):873–8.
[34] Germec M, Gürler HN, Ozcan A, Erkan SB, Karahalil E, Turhan I. Medium optimization and kinetic modeling for the production of *Aspergillus niger* inulinase. Bioprocess Biosyst Eng 2020;43(2):217–32.
[35] Sunarno JN, Prasertsan P, Duangsuwan W, Kongjan P, Cheirsilp B. Mathematical modeling of ethanol production from glycerol by *Enterobacter aerogenes* concerning the influence of impurities, substrate, and product concentration. Biochem Eng J 2020;155:107471.
[36] Phukoetphim N, Salakkam A, Laopaiboon P, Laopaiboon L. Kinetic models for batch ethanol production from sweet sorghum juice under normal and high gravity fermentations: logistic and modified Gompertz models. J Biotechnol 2017;243:69–75.
[37] Balakrishnan R, Tadi SRR, Rajaram SK, Mohan N, Sivaprakasam S. Batch and fed-batch fermentation of optically pure D (−) lactic acid from Kodo millet (*Paspalum scrobiculatum*) bran residue hydrolysate: growth and inhibition kinetic modeling. Prep Biochem Biotechnol 2020;50(4):365–78.
[38] Lim J, Byun HE, Kim B, Park H, Lee JH. Mathematical modeling of acetone–butanol–ethanol fermentation with simultaneous utilization of glucose and xylose by recombinant *Clostridium acetobutylicum*. Energy Fuels 2019;33(9):8620–31.
[39] Zheng Z, Chen Y, Zhan X, Gao M, Wang Z. Mass transfer intensification in a novel airlift reactor assembly with helical sieve plates. Chem Eng J 2018;342:61–70.

[40] Salehpour R, Jalilnejad E, Nalband M, Ghasemzadeh K. Hydrodynamic behavior of an airlift reactor with net draft tube withdifferent configurations: numerical evaluation using CFD technique. Particuology 2020;51:91–108.
[41] Li X, Chen Y, Zheng Z, Gao M, Wang Z, Zhang K, et al. Power-saving airlift bioreactor with helical sieveplates: developmental and performance studies. Chem Eng Res Des 2020;158:1–11.
[42] Han M, Laari A, Koiranen T. Effect of aeration mode on the performance of center- and annulus-rising internal-loop airlift bioreactors. Can J Chem Eng 2018;96(1):367–76.
[43] Rosa EAR, Bianchini LF, da Silva Ramos RCP, Arantes AB, da Silva RF, Glassey J. Hydrodynamics of split-rectangle-internal loop airlift bioreactor with variations in riser and downcomer cross-sectional areas based on the golden ratio. J Chem Technol Biotechnol 2019;94(4):1323–9.
[44] Kumar N, Gupta R, Bansal A. Effect of surface tension on hydrodynamics and mass transfer coefficient in airlift reactors. Chem Eng Technol 2020;43 (5):995–1004.
[45] Magdouli S, Brar SK, Blais JF. Morphology and rheological behaviour of *Yarrowia lipolytica*: impact of dissolved oxygen level on cell growth and lipid composition. Process Biochem 2018;65:1–10.
[46] Bull DN, Young MD. Enhanced product formation in continuous fermentations with microbial cell recycle. Biotechnol Bioeng 1981;23(2):373–89.
[47] Pappu JSM, Gummadi SN. Modeling and simulation of xylitol production in bioreactor by *Debaryomyces nepalensis* NCYC 3413 using unstructured and artificial neural network models. Bioresour Technol 2016;220:490–9.
[48] Chang G, Gao N, Tian G, Wu Q, Chang M, Wang X. Improvement of docosahexaenoic acid production on glycerol by *Schizochytrium* sp. S31 with constantly high oxygen transfer coefficient. Bioresour Technol 2013;142:400–6.
[49] Yamada R, Nishikawa R, Wakita K, Ogino H. Rapid and stable production of 2,3-butanediol by an engineered *Saccharomyces cerevisiae* strain in a continuous airlift bioreactor. J Ind Microbiol Biotechnol 2018;45(5):305–11.
[50] Sung MG, Lee B, Kim CW, Nam K, Chang YK. Enhancement of lipid productivity by adopting multi-stage continuous cultivation strategy in *Nannochloropsis gaditana*. Bioresour Technol 2017;229:20–5.
[51] Maitra S, Narang A. Existence of a scaling relation in continuous cultures of *Scheffersomyces stipitis*: the steady states are completely determined by the ratio of carbon and oxygen uptake rates. Biotechnol Biofuels 2019;12 (1):19.